

Resonance and phase shift in an open Aharonov–Bohm ring with an embedded quantum dot

Eric R Hedin¹, Yong S Joe¹ and Arkady M Satanin²

¹ Center for Computational Nanoscience, Department of Physics and Astronomy, Ball State University, Muncie, IN 47306, USA

² Institute for Physics of Microstructures, RAS, GSP-105, Nizhny Novgorod, 603950, Russia

Received 8 July 2008, in final form 31 October 2008

Published 2 December 2008

Online at stacks.iop.org/JPhysCM/21/015303

Abstract

The transmission and phase properties of electron transport through a quantum dot (QD) with variable coupling to a third-terminal probe are investigated analytically for the case of the QD connected directly to source and drain reservoirs and when the QD is embedded in one arm of an Aharonov–Bohm (AB) ring. Using the tight-binding model, explicit analytical expressions of the transmission through the QD for each case are given. Expressions for the conductance with coupling to the third terminal, which breaks unitarity and phase-locking, are also given. It is shown that in a three-terminal interferometer the zero of the Fano resonance in the transmission moves off the real energy axis for finite values of the coupling parameter. The zero orbits around the pole in the complex energy plane as a function of magnetic flux through the ring, and can be returned to the real energy axis unless the coupling parameter exceeds a critical value. With the QD embedded in one arm of the AB ring, the electron transmission and the transmission phase, and the phase of the AB oscillations, are described in relation to the degree of coupling to the third-terminal probe which opens the interferometer. By tuning the degree of coupling to the probe, it is shown that the phase of the AB oscillations can be made to match the intrinsic phase of the QD, facilitating experimental characterization of the phase response of the QD.

(Some figures in this article are in colour only in the electronic version)

1. Introduction

Quantum dots (QDs), or artificial atoms [1], when fabricated as a component of a meso-electronic system [2, 3] have important properties which affect their applications in nanotechnology devices. QDs have also been identified as prime candidates for applications in quantum computing and quantum information processing [4, 5]. It is well known that the quasi-bound state energy levels of the QD support transmission resonances of the Breit–Wigner form when the QD is part of a one-dimensional conductor. Fano-type resonances, characterized by an adjacent zero-pole pair, occur when the QD is inserted in one arm of an Aharonov–Bohm (AB) ring [6]. The continuum path through the reference arm of the ring provides interference with the electron wave through the arm containing the QD, resulting in the zero or one transmission states at particular electron energy values. The transmission through the QD has

been shown in this configuration to retain phase coherence, as demonstrated through the visibility of AB oscillations in the transmission as a function of magnetic flux applied perpendicularly the ring [7]. However, the exact transmission phase shift produced by the QD in the AB ring is not easily obtained by direct measurement. In a two-terminal device, the Onsager relations [8] of time-reversal symmetry and current conservation (unitarity) constrain the transmission phase to values of 0 or π . Measurements of the transmission phase in a two-terminal device (as determined by the phase of the AB oscillations) show flat phase dependence as a function of energy, except at the position of the resonance where the phase abruptly jumps by π [9, 10]. Thus, the true phase shift of the transmission through the QD is masked in a two-terminal device. However, if the two-terminal AB ring is ‘opened’ by coupling to additional terminals, the unitarity condition is broken and it becomes possible in principle to extract

meaningful phase information about the QD [9]. Analysis has shown that the measurable transmission phase in this case only matches the intrinsic phase of the QD under specific conditions relating to exactly how the AB ring is opened [11, 12]. We present here a theoretically simpler means by which the AB oscillation phase for an open ring can be tuned to match the intrinsic phase of the QD. Other mechanisms which have been postulated to contribute to the disruption of unitarity include QD inter-level thermal excitation and inelastic electron–phonon interactions [13].

We use a tight-binding model to analyze the transmission, conductance and phase properties of two- and three-terminal QDs connected to uniform conducting leads, or with the QD embedded in one arm of an AB interferometer. The tight-binding model has also been applied to transport analysis through coupled QDs considered as components of a biomolecular structure such as DNA [14]. The resonant transmission and phase properties of the electron transport through the QDs and AB rings described here provide additional theoretical understanding for these important applications. We show how the transmission and phase behavior through the QD varies with coupling to a third terminal, both as a bare three-terminal QD in a one-dimensional array (coupling through the reference arm of the AB ring blocked), and when the QD is embedded in one arm of the AB ring. It is seen that the zero of the Fano resonance produced by the QD and the ring leaves the real energy axis as coupling to the third terminal, V_d , is increased from zero. Other recent research on the mesoscopic Fano effect shows that for the case of imperfect coupling between the arms of the AB interferometer the transmission consists of mixed modes, which inhibit the complete destructive interference characteristic of the Fano resonance zero [15]. In the research presented here, however, we focus on the case of complete coupling between the AB arms.

When the ring is opened by coupling to the third terminal, the sudden phase jump of π is seen to soften. An expression for the transmission amplitude through the QD is $t = \sqrt{T_{\text{QD}}} e^{i\alpha_{\text{QD}}}$, which is a complex quantity. The intrinsic phase of the QD, α_{QD} , can be extracted from measurements of the phase of the AB oscillations with an open ring [9]. In our analysis, the intrinsic phase behavior of the QD (α_{QD}) is found to match the phase of the AB oscillations by uniquely tuning the coupling of the AB ring to the third terminal, thus providing a possible novel method of experimentally determining α_{QD} .

In addition, the behavior of the Fano zero and pole in the complex energy plane as a function of magnetic flux through the ring is analyzed. The zero orbits the pole with a periodicity equal to the flux quantum. In the case of an open ring, however, due to the zero-pole Fano dipole pair being shifted away from the real energy axis, the pole crosses the axis at values of flux which depart from the nominal zero-crossing values of $n\Phi_0/2$ ($n = 0, 1, 2, \dots$), where $\Phi_0 = h/e$ is the elementary flux quantum [16]. For values of flux which position the Fano zero in the positive complex energy half-plane, we can move the zero back across the real energy axis by sufficiently increasing the value of V_d . Experiments have shown a slight flux dependence of the transmission resonances

and the phase of the AB oscillations [17, 18]. However, this effect is insignificant if the area of the QD is small compared to the ring area (as assumed here), or for the case of weak fields [19].

Electron–electron interactions can add complicating features to the resonance and phase behavior of QDs in AB rings. However, as is customary for a simple lattice model, using the tight-binding approximation, electron–electron interactions are ignored or incorporated into the onsite energy of the QD [20]. The model then becomes a single-electron scattering case, which generally applies near a Coulomb blockade resonance where the interaction effect only provides a shift of the QD energy. Our focus is in this regime. We also assume the temperature, $T \rightarrow 0$ K, for which case Aharony *et al* have shown that the transmission resonance is completely determined according to non-interaction contributions [21, 22]. Kondo correlations between the unpaired spin of a single electron in the QD and the electrons in the leads can produce enhanced conduction in the valley between two Coulomb blockade peaks. These correlations have also been seen to diminish the phase lapse behavior of the QD across the Kondo valley [23]. Although our model is limited to discussions in which there is no electron–electron interaction, it is well known that the single-electron picture gives a qualitative and correct description of Fano resonances in atomic systems, and may be substantiated by using a self-consistent approximation.

It is well known that for a nano-ring it is difficult to separate the effect of the measurement probes from the measurement itself. Our theoretical model also demonstrates what kind of information may be extracted from three-terminal measurements. The analytical model of the QD and AB ring is presented next, followed by the transmission analysis and the phase behavior of the system.

2. Model of the QD and AB ring

We consider a special interferometer with an embedded QD in one arm and connected to a plunger (or probing) wire defining the outgoing reservoir (see figure 1). Besides current leads 1 and 2, the probing lead is connected with the QD directly in order to extract information regarding waves scattering on the QD. We analyze the system under consideration with a tight-binding model, which is equivalent to the discretized Schrödinger equation [24]. Numerous authors have employed this approximation to the Schrödinger equation in order to obtain analytical solutions for mesoscopic systems. Denoting the wavefunction on site n by ψ_n , the Schrödinger equation in the tight-binding approximation is

$$-\sum V_{n,m}\psi_m + \varepsilon_n\psi_n = E\psi_n, \quad (1)$$

where the sum runs over the nearest neighbors of n , E is the electron energy, and ε_n is the site energy. The parameters, $V_{n,m}$, are overlap integrals, or coupling parameters, involving the overlap of the single-site, atomic-like wavefunctions from sites m and n with the single-site potential of site n . In the homogeneous leads, the coupling parameters are all set to $V_0 = 1.0$, which we use throughout the discussion as a unit

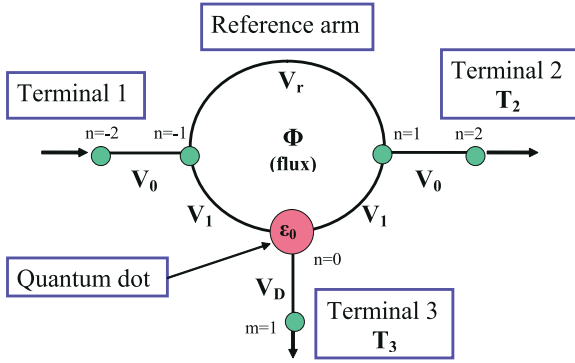


Figure 1. Schematic diagram of the quantum dot embedded in the AB ring with relevant coupling parameters between sites. V_1 sets the confinement of the QD, V_d allows coupling to the third terminal, and V_r provides coupling through the reference arm of the ring.

of energy. It is assumed that the electron–electron interaction is neglected in our calculations.

For the one-dimensional periodic potential lattice of the leads, the electron wavefunction is of the form $\psi_n = A e^{i\theta n} + B e^{-i\theta n}$, where the index n runs over all the sites of the perfect conductors and A and B are arbitrary amplitudes. Let us consider an incoming wavefunction only in the first wire

$$\psi_n = e^{i\theta n} + r_{11} e^{-i\theta n}, \quad n \leq -1, \quad (2)$$

where $\theta = ka$, a is the distance between the sites, k is the wavevector that is connected with the energy by the dispersion relation, $E = -2V_0 \cos ka$, and r_{11} is the reflection amplitude. The incoming wave produces outgoing waves in the second lead

$$\psi_n = t_{21} e^{i\theta n}, \quad n \geq 1, \quad (2.1)$$

and in the third lead

$$\psi_m = t_{31} e^{im\theta}, \quad m \geq 1, \quad (2.2)$$

where t_{21} and t_{31} are the transmission amplitudes into terminal 2 or 3 from the first lead. The site energies, ε_n , are set to zero for all sites except for the QD at $m = 0$, which has site energy ε_0 .

The flux through the ring produces a phase difference between the path through the QD and the path through the reference arm by the AB effect [25]. We choose a gauge in which the coupling parameter for each segment of the lower arm is modified as $V_1 \rightarrow V_1 e^{\pm i\varphi}$, and the reference arm coupling parameter becomes $V_r e^{\pm 2i\varphi}$ (‘+’ for counterclockwise transits around the ring and ‘-’ for clockwise transits). The phase, φ , is related to the magnetic flux, Φ , by $\varphi = \pi\Phi/(2\Phi_0)$. Wavefunction coupling to the third terminal is allowed for $V_d \neq 0$.

Applying equation (1) to the three sites around the AB ring and also to site $m = 1$ of the third terminal, we obtain the following three linear equations which are subsequently solved simultaneously for the complex reflection and transmission

amplitudes:

$$\begin{aligned} V_0 r_{11} - V_r e^{-2i\varphi+i\theta} t_{21} - \frac{V_1 V_0}{V_d} e^{i\varphi} t_{31} &= -V_0, \\ -V_r e^{2i\varphi+i\theta} r_{11} + V_0 t_{21} - \frac{V_1 V_0}{V_d} e^{-i\varphi} t_{31} &= V_r e^{2i\varphi-i\theta}, \\ -V_1 r_{11} e^{-i\varphi+i\theta} - V_1 t_{21} e^{i\varphi+i\theta} - \left(V_d e^{i\theta} - \frac{(\varepsilon_0 - E)V_0}{V_d} \right) t_{31} &= V_1 e^{-i\varphi-i\theta}. \end{aligned} \quad (3)$$

An explicit solution for unknown amplitudes may be found by inverting the matrix of coefficients of the reflection and transmission amplitudes on the left side of equation (3). The requirement of current conservation provides a check on the results through the relation

$$|r_{11}|^2 + |t_{21}|^2 + |t_{31}|^2 = 1. \quad (4)$$

In the same way we can find all the transmission t_{ij} and reflection r_{ij} amplitudes of the three terminal system. We then determine the probabilities: $T_{ij} = |t_{ij}|^2$ and $R_{ij} = |r_{ij}|^2$, which let us define the conductance of the network, as outlined below. Chemical potentials, μ_i , are applied to the nodes to produce the currents I_i in the leads [26]:

$$I_i = \frac{2e}{h} \left[(1 - R_{ii})\mu_i - \sum_{j \neq i} T_{ij}\mu_j \right]. \quad (5)$$

To find the non-local conductance we need to consider current conservation, $1 - R_{ii} = \sum_{j \neq i} T_{ij}$. For our purposes here, we set the current between nodes 1 and 2 as $I_1 = -I_2$. Firstly, we will be interested in how to measure the potential drop between nodes 1 and 2: $V_{12} = (\mu_1 - \mu_2)/e = I_1/G_{12,12}$, when the net current flowing to node 3 is considered negligible ($I_3 = 0$). The conductance $G_{12,12}$ is for the case of current from node 1 to node 2 (first set of subscripts), with the potential drop also measured between nodes 1 and 2 (second set of coefficients), using Büttiker’s notation [26]. We obtain an expression for this conductance in terms of the multi-terminal transmission coefficients as follows. Using equation (5), we write

$$\begin{aligned} I \equiv I_1 &= \frac{2e}{h} [(T_{12} + T_{13})\mu_1 - T_{12}\mu_2 - T_{13}\mu_3] = -I_2 \\ &= -\frac{2e}{h} [(T_{21} + T_{23})\mu_2 - T_{21}\mu_1 - T_{23}\mu_3]. \end{aligned} \quad (6)$$

To eliminate μ_3 we use $I_3 = 0$ to obtain $\mu_3 = (T_{31}\mu_1 + T_{32}\mu_2)/(T_{31} + T_{32})$. From here, there is more than one equivalent way to proceed; we choose to substitute the above expression for μ_3 into the expression for I_2 in equation (6). Then, without loss of generality [27], we set $\mu_2 = 0$ to obtain $I = I_1 = -I_2 = G_{12,12}(\mu_1/e)$, where

$$G_{12,12} = \frac{2e^2}{h} \left(T_{21} + \frac{T_{23}T_{31}}{T_{31} + T_{32}} \right). \quad (7)$$

The potential drop between nodes 3 and 2 is defined by the conductance

$$G_{12,32} = \frac{2e^2}{h} \left(T_{21} + T_{32} + \frac{T_{23}T_{31}}{T_{31}} \right), \quad (8)$$

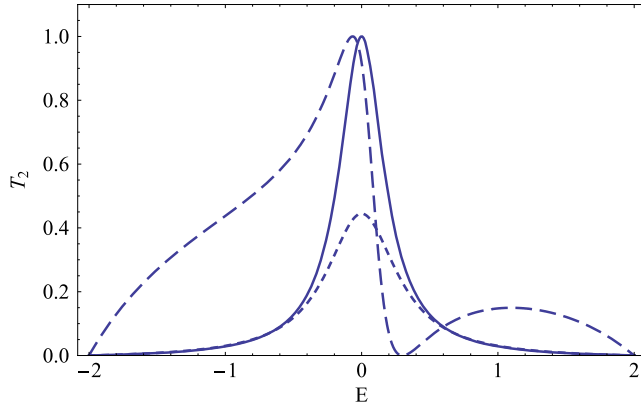


Figure 2. Transmission as a function of energy through a two-terminal QD (solid curve), a three-terminal QD ($V_d = 0.3$; dotted curve), and a two-terminal QD embedded in an AB ring ($V_d = 0$, $V_r = 0.3$; dashed curve).

obtained by a similar derivation. If coupling to the probing terminal 3 is blocked ($V_d = 0$), the conductance expressions above reduce to the familiar Landauer—Büttiker relation: $G = \frac{2e^2}{h} T_{21}$.

It is well known that in a magnetic field, current conservation and time-reversal invariance reads

$$T_{ij}(\Phi) = T_{ji}(-\Phi). \quad (9)$$

We will discuss in the next sections the behavior of the transmissions and conductance in an AB ring. Explicit, analytical solutions of the system of equations in (3) are presented in the following section for the case of a two-terminal QD, a three-terminal QD, the QD in a two-terminal AB ring, and the QD in a three-terminal AB ring.

3. Analytical results and discussion of the transmission

3.1. Two- or three-terminal QD

The simplest case is the two-terminal QD in a one-dimensional array, which is represented by setting $V_d = 0$ and $V_r = 0$ in figure 1. In this case, the transmission amplitude through the dot is given as

$$t_{21} = \frac{ig\sqrt{4V_0^2 - E^2}}{E - \frac{\varepsilon_0}{1-v^2} + ig\sqrt{4V_0^2 - E^2}}, \quad (10)$$

where $g = v^2/(1 - v^2)$ and $v = V_1/V_0$. A plot of the transmission through the QD as a function of energy is shown in figure 2 (solid curve). For all the graphical results presented below, $V_1 = 0.3$ for the QD confinement, and $V_r = 0.3$ when the QD is embedded in the AB ring. The site energy of the QD is taken as $\varepsilon_0 = 0$, which positions the resonance in the center of the allowed energy band. The external magnetic flux is set to zero, except where specified as a variable.

The coupling of the resonance with the propagating states is defined by parameter v . When the coupling parameter

is small, $v \ll 1$, the expression in equation (10) can be written approximately in the form of a standard Breit–Wigner resonance,

$$t_{21}(E) = \frac{i\Gamma}{E - E_p + i\Gamma}. \quad (11)$$

We find then the position of the resonance peak, $E_p = \varepsilon_0(1 - v^2)^{-1}$, which lies close to ε_0 for $v \ll 1$, or $V_1 \ll V_0$. Here, 2Γ is the full width at half maximum (FWHM) of the resonance with the parameter Γ approximately given as $\Gamma \cong g\sqrt{4V_0^2 - E_p^2}$.

We next consider the effect of adding a third terminal to the QD, which is represented by allowing $V_d \neq 0$, but still holding $V_r = 0$. The transmission amplitude for this case is given by

$$t_{21} = \frac{ig'(v/v')^2\sqrt{4V_0^2 - E^2}}{E - \frac{\varepsilon_0}{1-v^2} + ig'\sqrt{4V_0^2 - E^2}}, \quad (12)$$

where $g' = v^2/(1 - v'^2)$, $v' = \sqrt{v^2 + v_d^2/2}$, $v_d = V_d/V_0$ and is also plotted in figure 2 (dotted line). (Similarly, the transmission amplitude through the third terminal of the QD is simply related to t_{21} by $t_{31} = t_{21}(V_d/V_1)$.) The position of the resonance peak in the transmission through the three-terminal QD is now given by

$$E'_p = \frac{\varepsilon_0}{1 - (V_1^2 + V_d^2/2)/V_0^2} = \frac{\varepsilon_0}{1 - (v^2 + v_d^2/2)}. \quad (13)$$

The width of the resonance may be found by perturbation. We shall discuss a simple case when the coupling to the third lead is weak: $v_d \ll 1$, or $V_d \ll V_0$. With non-zero coupling to the third terminal, $V_d \neq 0$, the resonance peak is shifted slightly further to the outside of ε_0 (for $\varepsilon_0 \neq 0$), compared to the two-terminal case shown above. Not only is the position shifted, but the amplitude of the resonance peak falls below unity with non-zero V_d since there is then finite transmission to the third terminal. The transmission resonance through the three-terminal QD is no longer strictly of the Breit–Wigner form shown in equation (11), but it can be written as

$$t_{21}(E) = \frac{i(v/v')^2\Gamma'}{E - E'_p + i\Gamma'}. \quad (14)$$

The result of perturbation analysis gives the width of the resonance approximately as $\Gamma' \cong g'\sqrt{4V_0^2 - E_p'^2}$. Notice that since $v \ll v'$ the imaginary part of the denominator of equation (14) is now greater than the imaginary part of the numerator. The increased imaginary part of the resonance pole indicates an increased width of the resonance, which is related to the shorter lifetime of the resonance state of the QD due to leakage current into the open third terminal. We find that the magnitude of the transmission to the second terminal at the resonance peak for the three-terminal QD is

$$T_{21}(E'_p) = (v/v')^4 = \frac{V_1^4}{(V_1^2 + V_d^2/2)^2} < 1. \quad (15)$$

We see that the effect of adding the third terminal to the QD changes the transmission dramatically: we can treat the effect of the additional terminal as a source of inelastic processes because the electrons that are transmitted to third lead lose their phase coherence.

3.2. QD embedded in an AB ring

When coupling through the reference arm is allowed ($V_r \neq 0$), the QD is effectively embedded into one arm of an AB interferometer ring. In order to simplify notation, from here on, T_2 and t_2 will represent the transmission and transmission amplitude, respectively, from terminal 1 into terminal 2. We first present the case of a two-terminal ring, obtained by setting $V_d = 0$. The transmission amplitude is then found to be

$$t_2 = \{2i \sin \theta [V_1^2 - e^{4i\varphi} V_r (E - \varepsilon_0)] \{e^{2i\theta} V_r V_1^2 (e^{6i\varphi} + e^{-2i\varphi}) / V_0 + e^{2i\varphi} [2V_1^2 e^{i\theta} + (E - \varepsilon_0) \times (V_0 - e^{2i\theta} V_r^2 / V_0)]\}^{-1}. \quad (16)$$

Due to the additional reference arm path, interference between the continuum modes and the quasi-bound state of the QD shifts the form of the resonance from a Breit–Wigner to a Fano resonance, with its zero-pole pair characteristics as seen in figure 2 (dashed line). With the Fano resonances, the behavior of the Fano zero becomes of primary interest to us. The position of the resonance zero is easily obtained by solving for the value of the energy, E_0 , which causes the numerator of t_2 to be zero. This is found from equation (16) to be $E_0 = \varepsilon_0 + e^{-4i\varphi} V_1^2 / V_r$. For zero flux (or, for $4\varphi = n\pi$, $n = 0, 1, 2, \dots$), the resonance zero always lies on the real energy axis in a two-terminal AB ring. The phase behavior for each transmission curve shown in figure 2 is presented in figure 5, and is discussed below in section 4.

Next, we present the case of a three-terminal ring with $V_d \neq 0$. The expression for the full transmission amplitude is now written as

$$t_2 = \{2i \sin \theta [V_1^2 - e^{4i\varphi} V_r (E - \varepsilon_0 + e^{i\theta} V_d^2 / V_0)] \times \{e^{2i\theta} V_r V_1^2 (e^{6i\varphi} + e^{-2i\varphi}) / V_0 + e^{2i\varphi} [(2V_1^2 + V_d^2) e^{i\theta} - e^{3i\theta} V_r^2 V_d^2 / V_0^2 + (E - \varepsilon_0)(V_0 - e^{2i\theta} V_r^2 / V_0)]\}^{-1}. \quad (17)$$

Plots of the transmission versus energy for various values of coupling, V_d , to the third terminal are shown in figure 3. Opening the ring, by allowing non-zero V_d , immediately shifts the Fano zero off the real energy axis into the complex energy plane (see both the dotted and dashed lines in figure 3). However, for each value of V_d (up to a critical value described below) there exist two values of magnetic flux for which the Fano zero can again be positioned back on the real energy axis. By setting the term in square brackets in the numerator of equation (17) to zero, we obtain the following two equations, which can be solved simultaneously to give the energy, E_0 , and corresponding magnetic flux values which force the transmission to be zero:

$$E_0 = \frac{2V_0^2 [\varepsilon_0 + (V_1^2 / V_r) \cos 4\varphi]}{2V_0^2 - V_d^2} \quad (18)$$

$$\text{and} \quad E_0 = \pm 2V_0 \sqrt{1 - \frac{V_1^4 V_0^2}{V_r^2 V_d^4} \sin^2 4\varphi}.$$

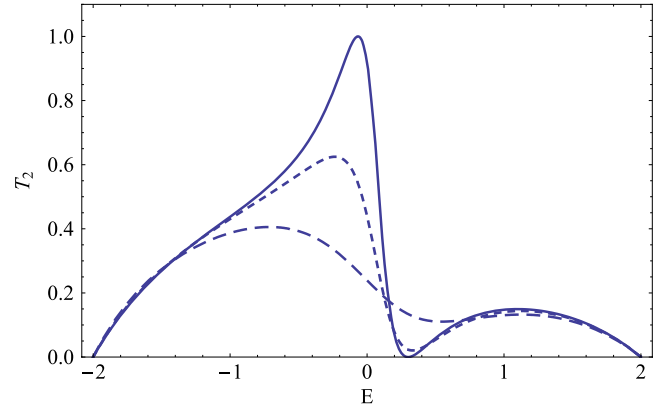


Figure 3. Transmission through the ring into the second terminal as a function of energy, for a closed ring ($V_d = 0$, solid curve) and for open rings ($V_d = 0.3$, dotted curve; $V_d = 0.6$, dashed curve). The Fano zero lifts off the real energy axis for non-zero coupling to the third terminal of the ring.

The two conditions in equation (18) follow from requiring both the real and the imaginary parts of the numerator of equation (17) to be zero. In the case with $\varepsilon_0 = 0$, it is possible to obtain simple, closed forms for E_0 and the flux in terms of the coupling parameters [16].

A critical value of V_d exists ($V_d^{\text{crit}} = V_1 \sqrt{V_0 / V_r}$), which is the maximum value for which there is the possibility of placing the Fano zero on the real energy axis at any value of flux. For the parameters used in this section ($V_0 = 1.0$ and $V_1 = V_r = 0.3$), the critical value becomes $V_d^{\text{crit}} = \sqrt{0.3} \cong 0.5477$ [16]. In figure 4, we show the transmission T_2 as a function of electron energy (the left column) and contour plots of the transmission amplitude in the complex energy plane (the right column) with fixed magnetic flux $\Phi / \Phi_0 = 0.75$ for three different values of $V_d = 0.3, 0.548$ and 0.8 . As V_d increases, the Fano zero moves directly downward and crosses the real energy axis at V_d^{crit} . If V_d is increased beyond V_d^{crit} , the Fano zero passes into the negative complex energy half-plane and there is no value of flux which can bring the Fano zero back to the real energy axis.

4. Phase analysis of the transmission and AB oscillation

4.1. Two- or three-terminal QD

For a two-terminal symmetric QD in a one-dimensional periodic lattice (modeled in our analysis by setting $V_r = 0$ and $V_d = 0$), the unitary scattering matrix connecting the transmission and reflection amplitudes on either side of the dot can be written as $S_2 = \begin{pmatrix} t^{-1} & t \\ t & t^{-1} \end{pmatrix}$, where t is the transmission amplitude from either direction, and is given by equation (10) for the tight-binding model used in our calculations. The reflection amplitude is $r = t - 1$. The condition of unitarity, $S_2^{-1} = \tilde{S}_2^*$ (inverse equals conjugate transpose), requires in general that $|\det(S_2)|^2 = 1$, where $\det(S_2)$ is the determinant of matrix S_2 . Using the matrix form of S_2 given above, and expressing t as $t = \sqrt{T_{\text{QD}}} e^{i\alpha_{\text{QD}}}$, we find $\det(S_2) = -e^{2i\alpha_{\text{QD}}}$

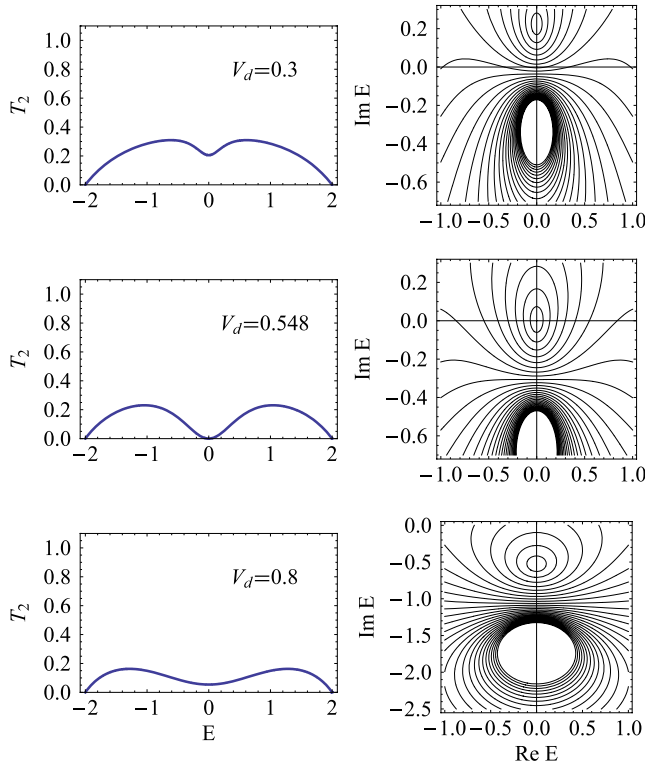


Figure 4. Transmission plots and contour plots of the transmission amplitude in the complex energy plane for $\Phi/\Phi_0 = 0.75$, showing the Fano zero crossing the real energy axis at the critical value of the coupling parameter, $V_d^{\text{crit}} = \sqrt{0.3} \cong 0.548$. For $V_d > V_d^{\text{crit}}$, the Fano zero passes into the negative complex energy half-plane, and cannot be returned to the real energy axis for any value of magnetic flux.

and $\sqrt{T_{\text{QD}}} = \cos(\alpha_{\text{QD}})$. Thus, for this case, the intrinsic phase of the QD can be obtained directly from the measured transmission current, shown in figure 5 (solid curve), in which the phase smoothly increases from $-\pi/2$ to $\pi/2$ across the resonance. The expression, $\sqrt{T_{\text{QD}}} = \cos(\alpha_{\text{QD}})$, is equivalent to $T_{\text{QD}} = \text{Re}(t)$, which holds for the general form of a Breit–Wigner transmission resonance, equation (11), but not for the Fano-type resonance which arises when the QD is embedded in one arm of an AB ring. Allowing additional loss from the QD by coupling to a third terminal only slightly modifies the transmission phase (of terminal 2), as seen in figure 5 for $V_d = 0.3$ (dotted curve). The phase of the transmission out of the third terminal of the QD (when not embedded in the AB ring) is identical to the transmission phase from the second terminal, even though the transmission amplitudes themselves differ, as shown in section 3.2 ($t_3 = t_2 V_d/V_1$).

4.2. QD embedded in a closed AB ring

When the QD is embedded in one arm of a two-terminal AB ring, the resulting Fano resonance in the transmission T_2 is accompanied by a transmission phase shift which shows a sharp phase jump of π for $V_d = 0$ (see dashed curve in figure 5). Experimentally, this sudden phase jump can be observed in the measurement of the phase of the AB oscillations [7, 9]. Figure 6(a) shows the analytically

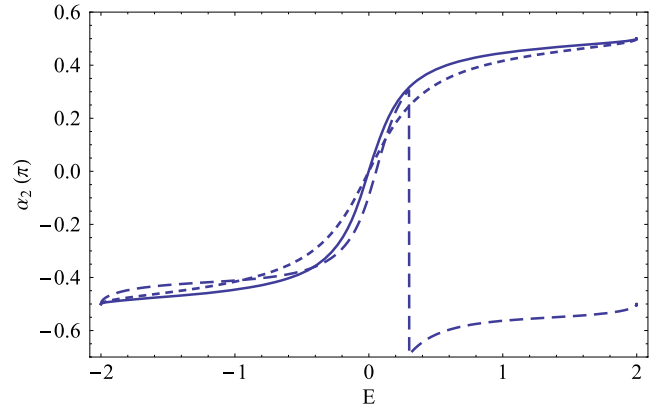


Figure 5. Transmission phase as a function of energy through a two-terminal QD (solid curve), a three-terminal QD ($V_d = 0.3$; dotted curve), and a two-terminal QD embedded in an AB ring ($V_d = 0$, $V_r = 0.3$; dashed curve). The phase jumps abruptly by π for the QD in one arm of the AB ring.

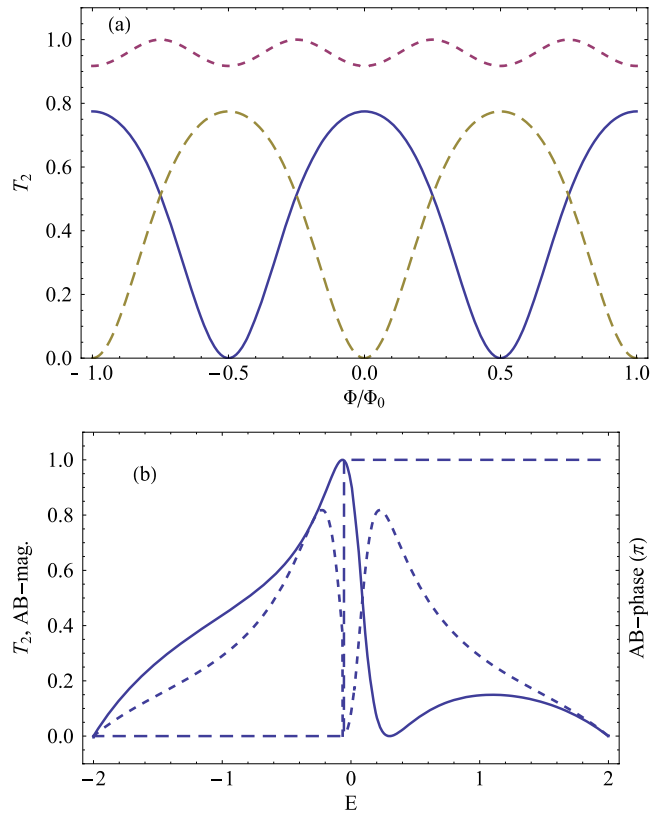


Figure 6. (a) Transmission as a function of magnetic flux for the closed ring, showing the phase shift of the AB oscillations for energy values on either side of the resonance. Solid curve, $E = -0.3$; dotted curve, $E = 0.0$; dashed curve, $E = 0.3$. (b) Transmission and AB oscillation amplitude and phase as a function of energy for the closed ring. Solid curve, T_2 versus E ; dotted curve, AB oscillation amplitude; dashed curve, AB oscillation phase, showing the sharp phase jump of π at the Fano resonance peak.

calculated AB oscillations at three specific energy values across the resonance, and figure 6(b) plots the magnitude and phase of the AB oscillations, along with the Fano transmission resonance as a function of energy. The sharp phase jump of

π in the AB phase at the resonance peak is clearly exhibited in figure 6(b) (dashed curve). In our analytical results, the complex transmission amplitude for the AB ring with the embedded QD can be expressed as $t_2 = |t_2| e^{i\alpha_2}$, giving the transmission phase as $\alpha_2 = \arctan[\text{Im}(t_2)/\text{Re}(t_2)]$. The explanation for the phase rigidity seen in the AB oscillations can be understood by writing t_2 as the sum of the transmissions through the two arms of the AB ring: $t_2 = |t_r| e^{i\alpha_r} + |t_d| e^{i\alpha_d} e^{i\phi}$. The subscripts ‘r’ and ‘d’ refer to the reference arm and to the arm with the QD, respectively. The phasor, $e^{i\alpha_d}$ includes the phase contribution of the QD, α_{QD} . The phasor, $e^{i\phi}$, is the contribution from the magnetic flux, Φ , where $\phi = 2\pi\Phi/\Phi_0$. The transmission, $T_2 = |t_2|^2$, is then sinusoidally dependent on the flux:

$$T_2 = |t_r|^2 + |t_d|^2 + 2|t_r||t_d| \cos(\alpha_r - \alpha_d + \phi). \quad (19)$$

Current conservation and time-reversal symmetry lead to the Onsager relation, which requires that the transmission must be an even function of the flux: $T_2(\Phi) = T_2(-\Phi)$ [27]. The only way for this to be true in general is if $\alpha_r - \alpha_d = 0, \pi$, which is seen analytically when the phase of the transmission through the closed ring exhibits a sharp jump of π at the resonance zero, as shown in figure 7 (solid curve). This phase rigidity of the closed AB ring ($V_d = 0$) masks the intrinsic phase of the QD, α_{QD} , preventing its measurement via the phase of the AB oscillations [7].

An analytical expression for the transmission through the two-terminal ring showing its flux dependence is given in equation (20) as $T_2 = |t_2|^2$, where t_2 is the transmission amplitude from equation (16). The flux dependence of equation (20) is more complicated than the result of the ideal interferometric model given in equation (19), since equation (19) assumes a single passage of the electron wave through the device, while equation (20) takes into account multiple (infinite) reflections from the QD scatterer and from the input and output junctions of the AB ring [20].

$$T_2 = \frac{4 \sin^2 \theta [V_1^2 + V_r^2 (E - \varepsilon_0)^2 - 2V_1^2 V_r (E - \varepsilon_0) \cos \phi]}{(V_1^2 V_r / V_0) [(V_1^2 V_r / V_0) 4 \cos^2 \phi + 2 \cos \phi (C + C^*)] + CC^*}. \quad (20)$$

Here, C is an energy-dependent factor; $C = 2V_1^2 e^{-i\theta} + (E - \varepsilon_0)(V_0 e^{-2i\theta} - V_r^2 / V_0)$. The transmission is seen to depend upon factors of both $\cos \phi$ and $\cos^2 \phi$, with the periodicity of the flux quantum ($\phi = 2\pi\Phi/\Phi_0$) being predominant at energies away from the resonance. At the energy of the resonance ($E = \varepsilon_0 = 0$), for our results, the transmission of equation (20) simplifies considerably to

$$T_2 = \frac{1}{(V_r^2 / V_0^2) \cos^2 \phi + 1}. \quad (21)$$

Here, the AB oscillations are periodic with half the flux quantum, and $T_2(\phi)$ has minima at $\phi = 2\pi\Phi/\Phi_0 = n\pi$ (for n an integer), as seen in figure 6(a) for $E = 0$ (dotted curve). Experiments which measure the AB oscillations also reveal a departure from a pure sinusoidal dependence of the

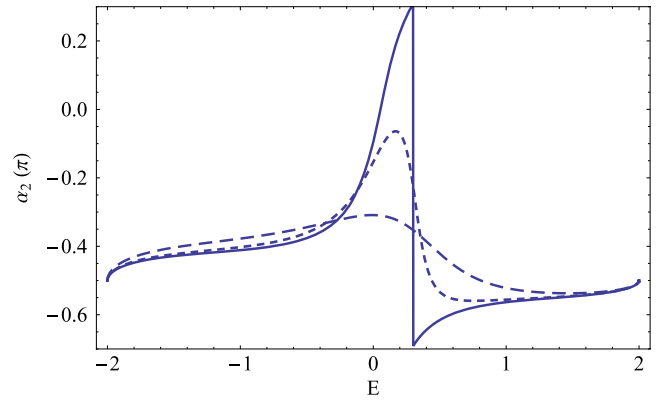


Figure 7. Transmission phase as a function of energy for the QD embedded in an AB ring. The phase jump of π at the transmission resonance zero (compare to figure 3) diminishes and softens as the ring is opened with coupling to the third terminal. $V_d = 0.0, 0.3$, and 0.6 (solid, dotted, and dashed curves, respectively).

transmission on the flux, with the dominant flux periodicity changing from Φ_0 to $\Phi_0/2$ at the resonance [28].

Aharony *et al* [20, 21] demonstrate that if coherence through the QD is assumed it is possible to indirectly extract α_{QD} from the transmission curve without opening the ring. However, their method employs a non-trivial five-parameter fit of the transmission under the condition of no flux-dependent internal electron–electron interactions. Below, in section 4.4, we show how to tune the three-terminal AB ring in order to obtain α_{QD} from the phase of the AB oscillations.

4.3. QD embedded in an open AB ring

In an open ring, the phase rigidity is removed, and the phase factor, $\alpha_r - \alpha_d \equiv \beta$, can smoothly vary across the resonance. As V_d increases from zero, allowing coupling and transmission to the third channel, unitarity is broken and the abrupt phase jump softens and decreases in magnitude [12, 21]. The transmission phase curves showing this effect for $V_d = 0.0, 0.3$, and 0.6 are plotted in figure 7. In order to experimentally extract the phase factor β , higher order harmonics of the flux dependence, as seen in the analytical result for the transmission through the closed ring, equation (20), are required to fit the measured conductance of an open ring to an ideal form of the transmission similar to that described above in equation (19). The factor, β , can then be determined from such a fit, but Aharony *et al* [11, 21] make the point that in an open AB interferometer with an embedded QD, the value of the parameter β is only equal to α_{QD} under certain conditions related to the details of the couplings to the extra terminals. In particular, they propose that if the AB ring is opened by moderate coupling to many extra terminals (‘combs’) placed around the ring, then it is possible to have $\alpha_{\text{QD}} = \beta$. If a loss channel is attached directly to the QD (as in our three-terminal case), Aharony *et al* find that β cannot be matched to α_{QD} , since β then changes by less than π across the resonance, while α_{QD} varies by π . This diminishing of the change in the phase factor β for loss directly from the QD suggests that β is in this case more closely characteristic of the *transmission* phase

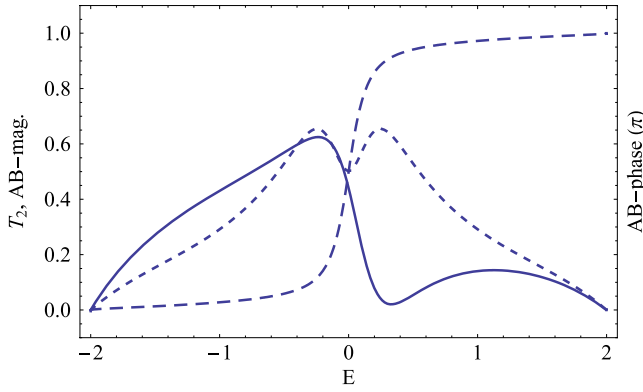


Figure 8. Transmission and AB oscillation amplitude and phase as a function of energy for the open ring ($V_d = 0.3$). T_2 versus E (solid curve); AB oscillation amplitude (dotted curve); AB oscillation phase (dashed curve).

change, rather than the AB phase, which varies as does α_{QD} by π across the resonance, even in an open ring. The transmission phase change, however, is shown to both soften and diminish to less than π in magnitude for an open ring with $V_d \neq 0$ (see figure 7). A simple analytical model of the transmission phase through the AB ring based on the properties of the Fano resonance in closed and open rings has been published by us in a recent paper related to this work [16]. This model illustrates both the phase jump and the softening effect brought on by coupling to the third terminal as a natural result of the Fano zero shifting from real to complex values as the ring is opened.

The transmission through a QD in an AB ring (given by the amplitude of the AB oscillations) has been shown experimentally to go to zero at the energy of the phase jump of the AB oscillations. This is seen in [9] to lie between the energy of the transmission zero and its peak, approximately at the energy, $E = E_R$, for the observed Fano resonance. Other work demonstrates that the phase jump in the transmission through the QD embedded in the two-terminal AB ring occurs at the transmission resonance peak [29]. This result is also seen directly in figure 6(b), in which the phase of the AB oscillations is plotted for the closed ring.

4.4. Tuning the AB phase to the intrinsic phase of the QD

When the ring is opened by allowing coupling to the third terminal, the intrinsic phase of the QD, α_{QD} , can in principle be obtained by measuring the phase shift of the AB oscillations, which is no longer forced by the Onsager relation to be 0 or π . Figure 8 shows plots of the transmission, and the magnitude and phase of the AB oscillations as a function of energy, for an open ring with $V_d = 0.3$. The AB phase here clearly exhibits the same form as the intrinsic phase of the QD shown in figure 5. We find that the AB phase of the open ring can be tuned to match the intrinsic phase of the two-terminal QD, α_{QD} (or the intrinsic phase of the three-terminal QD), by varying the degree of coupling to the third terminal of the AB ring. Figure 9 shows plots of the AB phase for $V_d = 0.3, 0.42, 0.51, 0.6,$ and 0.7 in comparison to α_{QD} for the two- and three-terminal QDs. The

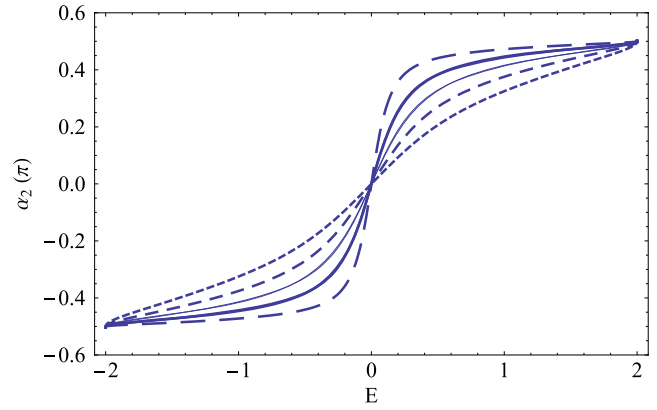


Figure 9. Transmission phase and AB oscillation phase plots. (i) Darker solid curve, transmission phase for a two-terminal QD ($V_d = 0, V_r = 0$), representing the intrinsic phase of the QD. The AB oscillation phase overlaps this curve for $V_d = V_d^{\text{QD}} = 0.42$. (ii) Lighter solid curve, transmission phase for a three-terminal QD ($V_d = 0.3, V_r = 0$). The AB oscillation phase overlaps this curve for $V_d = 0.51$. (iii) Dashed curves, AB oscillation phase for $V_d = 0.3, V_d = 0.6, V_d = 0.7$ (long dashes, short dashes, dotted, respectively).

AB phase for $V_d = 0.42$ matches the intrinsic phase of the two-terminal QD, and overlays α_{QD} in figure 9 (darker solid curve). An analytical solution for this particular value of V_d which tunes the AB phase to match α_{QD} is given below. At this specific value of the V_d , called V_d^{QD} , the loss current from the QD through the third terminal provides the conditions necessary to almost completely cancel the masking effect of the Onsager relations which force phase rigidity in a closed AB interferometer with current conservation. The open ring with $V_d = V_d^{\text{QD}}$ effectively acts like an ideal two-terminal AB interferometer in which the restrictive conditions on the AB phase due to current conservation and time-reversal symmetry are nullified, thus allowing the intrinsic phase contribution of the QD to be directly determined from the AB phase of this device. V_d^{QD} is found by analytically solving for the value of V_d which causes the AB phase to match α_{QD} at a particular value of energy between $E = 0$ and $\pm 2V_0$. The particular value of energy chosen is E_0 , which is the energy at which the Fano zero crosses the real energy axis at a specific value of magnetic flux (related to the AB phase) for a given set of coupling parameters. E_0 and the specific value of flux are found in terms of the coupling parameters from equation (18) [16]. Solving for the value of $V_d = V_d^{\text{QD}}$ which gives a match between the AB phase and $\alpha_{\text{QD}}(E)$ at $E = E_0$ yields $V_d^{\text{QD}} = \sqrt{2}V_1$. Since the form of the AB phase as a function of E is very close to $\alpha_{\text{QD}}(E)$, if these functions match at three points ($E = 0, E = \pm 2V_0$, and $E = E_0$), they closely match at all points in the allowed energy window ($-2V_0 \leq E \leq 2V_0$), especially for small V_1 or for $V_r \leq V_1$. Small V_1 provides greater confinement for the electrons in the QD, and $V_r \leq V_1$ guarantees that the arm of the AB ring containing the QD is not bypassed to too great an extent by the reference arm. Both of these conditions are necessary for the phase of the AB oscillations to sufficiently reflect the intrinsic phase contribution of the QD. In general, for a QD

defined by a given confinement parameter, V_1 , the intrinsic phase of this QD will closely match the AB phase of the three-terminal interferometer in which it is embedded if $V_f \leq V_1$, and $V_d = V_d^{\text{QD}} = \sqrt{2}V_1$. For $V_1 = 0.3$, $V_d^{\text{QD}} = 0.424$, which gives the overlapping curves for the AB phase and $\alpha_{\text{QD}}(E)$, shown in figure 9. Additionally, by further increasing V_d the AB phase can be made to match the intrinsic phase of the three-terminal QD, shown in figure 9 with the dotted curves for $V_d = 0.51$. This value of V_d can be determined empirically by adjusting V_d until the AB oscillation magnitude flattens out across $E = 0$. (The local minimum of the AB oscillation magnitude seen in figure 8 disappears for $V_d \geq 0.51$.)

In order to experimentally test the effect of nullifying the multiple reflections through the ring and QD, it would perhaps be desirable to fabricate an AB interferometer with smoothly tapering input and output Y-junctions in which single-mode propagation dominated without multiple reflections. The transmission and phase behavior of such a device should more closely match that of an ideal Mach–Zehnder interferometer, without the complicating effects of multiple reflections through the QD.

5. Conclusion

Using the exactly solvable formalism of the tight-binding model, we have presented analytical solutions for the transmission through an isolated two- and three-terminal QD and for a QD embedded in one arm of a two- or three-terminal AB interferometer. In the AB ring, coupling to the third terminal shifts the zero of the Fano transmission resonance into the complex energy plane. However, a unique interplay between the flux through the ring and coupling to the third terminal opens up a regime of parameter space where the Fano zero can be returned to the real energy axis even for the open AB ring. A critical maximum value of the third-terminal coupling parameter exists, however, above which there is no value of flux which can bring the Fano zero back to the real energy axis.

The exact analytical solutions also allow comparison of the behavior of the transmission phase to that obtained from a simple model based on the generic form of the Fano resonance. As the coupling to the third terminal is increased from zero, the phase jump seen at the resonance diminishes and softens. Additionally, by tuning the coupling to the third terminal of the AB ring, the phase of the AB oscillations can be made to match the intrinsic phase of the QD. By this method, the three-terminal AB ring with an embedded QD could be designed to experimentally obtain the intrinsic phase of the QD.

Acknowledgments

One of the authors (ERH) is partially supported by a grant from the Center for Energy Research, Education, and Service at Ball

State University. The work of YSJ is supported in part by the Enhanced Provost Initiative Fund at Ball State University.

References

- [1] Kastner M A 1993 *Phys. Today* **46** 24
- [2] Sigrist M, Ihn T, Ensslin K, Reinwald M and Wegscheider W 2007 *Phys. Rev. Lett.* **98** 036805
- [3] Holleitner A, Decker C, Qin H, Eberl K and Blick R 2001 *Phys. Rev. Lett.* **87** 256802
- [4] Loss D and DiVincenzo D 1998 *Phys. Rev. A* **57** 120
- [5] Olaya-Castro A and Johnson N 2005 *Quantum Information Processing in Nanostructures (Handbook of Theoretical and Computational Nanotechnology vol X)* ed M Rieth and W Schommers (Stevenson Ranch, CA: American Scientific Publishers)
- [6] Joe Y S, Kim J S, Hedin E R, Cosby R M and Satanin A M 2005 *J. Comput. Electron.* **4** 129
- [7] Yacoby A, Heiblum M, Mahalu D and Shtrikman H 1995 *Phys. Rev. Lett.* **74** 4047
- [8] Onsager L 1931 *Phys. Rev.* **38** 2265
- [9] Schuster R, Buks E, Heiblum M, Mahalu D, Umansky V and Shtrikman H 1997 *Nature* **385** 417
- [10] Katsumoto S, Kobayashi K, Aikawa H, Sano A and Iye Y 2003 *Superlatt. Microstruct.* **24** 151
- [11] Aharony A, Entin-Wohlman O, Halperin B I and Imry Y 2002 *Phys. Rev. B* **66** 115311
- [12] Entin-Wohlman O, Aharony A, Imry Y, Levinson Y and Schiller A 2002 *Phys. Rev. Lett.* **88** 166801
- [13] Yahalom A and Englman R 2006 *Phys. Rev. B* **74** 115328
- [14] Cuniberti G, Maciá E, Rodriguez A and Römer R A 2007 *Tight-binding modeling of charge migration in DNA devices Charge Migration in DNA: Perspectives from Physics, Chemistry, and Biology* ed T Chakraborty (Berlin: Springer)
- [15] Kubo T, Tokura Y, Hatano T and Tarucha S 2006 *Phys. Rev. B* **74** 205310
- [16] Joe Y S, Hedin E R and Satanin A M 2007 *Phys. Rev. B* **76** 085419
- [17] Aharony A, Entin-Wohlman O, Otsuka T, Katsumoto S, Aikawa H and Kobayashi K 2006 *Phys. Rev. B* **73** 195329
- [18] Kobayashi K, Aikawa H, Katsumoto S and Iye Y 2002 *Phys. Rev. Lett.* **88** 256806
- [19] Moldoveanu V, Tolea M, Gudmundsson V and Manolescu A 2005 *Phys. Rev. B* **72** 085338
- [20] Aharony A, Entin-Wohlman O and Imry Y 2003 *Phys. Rev. Lett.* **90** 156802
- [21] Aharony A, Entin-Wohlman O and Imry Y 2003 *Turk. J. Phys.* **27** 299
- [22] Aharony A, Entin-Wohlman O and Imry Y 2005 *Physica E* **29** 283
- [23] Ji Y, Heiblum M and Shtrikman H 2002 *Phys. Rev. Lett.* **88** 076601
- [24] Boykin T B and Klimeck G 2005 *Eur. J. Phys.* **26** 865
- [25] Aharonov Y and Bohm D 1959 *Phys. Rev.* **115** 485
- [26] Büttiker M 1986 *Phys. Rev. Lett.* **57** 1761
- [27] Datta S 1995 *Electronic Transport in Mesoscopic Systems* (Cambridge: Cambridge University Press)
- [28] Yacoby A, Schuster R and Heiblum M 1996 *Phys. Rev. B* **53** 9583
- [29] Wu J, Gu B-L, Chen H, Duan W and Kawazoe Y 1998 *Phys. Rev. Lett.* **80** 1952